Available online at www.sciencedirect.com

ScienceDirect

IFAC PapersOnLine 56-2 (2023) 7140–7146

Closed-loop Optimal Ageing-Aware Charging of Li-ion Batteries Using a Surrogate Model ⋆

D. Locatelli * **D.M. Raimondo** * **Z. Khalik** ** **H.J. Bergveld** ** **M.C.F. Donkers** **

* *Dept. of Electrical Engineering of University of Pavia, Italy (e-mail: diego.locatelli01@universitadipavia.it, davide.raimondo@unipv.it)*
** *Dept. of Electrical Engineering of Eindhoven University of Technology, Netherlands (e-mail: {z.khalik, h.j.bergveld, m.c.f.donkers}@tue.nl)*

Abstract: Li-ion batteries offer the finest balance of performance, price, and longevity for efficient energy storage. One of the main features of the Battery Management System (BMS) is to yield the best trade-off between fast charging and ageing effects minimisation while meeting safety requirements. In this paper, we provide an online optimal-control-based strategy for ageing-aware charging. This is achieved by formulating a control problem where a surrogate model is exploited in the description of the battery behaviour, that minimizes the side reactions, while satisfying ageing-related and safety constraints. The surrogate model combines a static nonlinear model that depends on the state of charge with a black-box finite-dimensional linear-time-invariant model. The results are obtained in simulation with a DFN battery model considered as a real "plant". To close the loop, a Kalman Filter with a forgetting factor is employed to estimate the states. Finally, we will compare the Pareto-fronts obtained using the suggested optimal-control-based methodology with those obtained using an open-loop strategy.

Keywords: Battery management system, Predictive control, Systems modeling, Li-ion Batteries.

1. INTRODUCTION

Lithium-based batteries demonstrate high energy efficiency, long cycle life, high energy and power density, and lack of memory effect, making them a popular energy storage solution. As a result, Li-ion batteries have emerged as the most prominent energy storage device, capturing significant attention due to their usage in electric vehicles, consumer electronics, and grid power storage.

One of the biggest challenges faced by battery-powered devices, particularly electrified vehicles, is charging time. For this reason fast charging is a crucial area of study since it improves usability and customer acceptance. However, it is important to note that the effectiveness of fast-charging strategies depends on the charging technique used, and some techniques may negatively impact battery longevity. Therefore, achieving a balance between fast charging and preserving battery life is essential. Fast charging, frequently entails high current rates, leading to high temperatures and high overpotentials which cause the early occurrence of a side-reaction. It is therefore important to find the best balance between battery ageing and charging time in order to provide a Pareto optimal trade-off (Khalik et al., 2020).

Rechargeable batteries are frequently charged using the Constant Current Constant Voltage (CC-CV) protocol. The charging protocol begins with a CC phase, which transitions to a CV phase once a specific voltage is reached. The CV phase ends when the current falls below a predefined threshold. The CC-CV charging protocol is a standard in the majority of applications due to its simplicity and ease of implementation. A trade-off between fast charging and a long cycle life can be obtained by tuning the values of the constant current in the CC phase and the constant voltage in CV phase. However, a significant disadvantage of this protocol is that the CV phase can result in long charging times, unless higher currents are used, which could compromise battery longevity. For this reason, literature has proposed some alternative protocols in order to be able to charging faster, without sacrificing cycle life.

The deploy of Multi Stage Constant Current (MSCC) protocols have been proposed in various studies, such as (Khan and Choi, 2018) and (Jiang et al., 2020), highlighting their importance in improving the longevity and performance of lithium-ion batteries. The effectiveness of pulse-charging protocols has been proven by Li et al. (2001) and Bhardwaj et al. (2014), where short rest inter-

⋆ This work received partial support from the Italian Ministry for Research (Grant no. 2017YKXYXJ), the Italian National Agency for New Technologies, Energy and Sustainable Economic Development (ENEA), and Regione Lombardia. Additionally, financial support was provided by the Dutch Ministry of Economic Affairs and Climate, under the grant 'R&D Mobility Sectors' carried out by the Dutch Enterprise Agency (RVO).

10.1016/j.ifacol.2023.10.593

vals or discharge pulses interrupt the charging current on a regular basis. These techniques try to minimise concentration polarisation and the possibility of negative local anode potential. Boost-charging algorithms are presented in Lee et al. (2021), where a high average current is followed by a CC-CV with lower currents, resulting in a reduced overall charging time. However, the above mentioned algorithms do not provide guarantees of optimality and have been developed based on the nominal chemical-physical cell characteristics.

Within this context, over the past few years, there has been a growing interest in model-based charging strategies. Several Li-ion cell models are available in the literature, including Equivalent-Circuit Models (ECMs) and Electrochemical Models (EMs). ECMs mainly describe macroscopic processes. For this reason they have few states and are hence ideal for real-time applications. EMs, on the other hand, accurately describe chemical processes occurring inside a cell, at the price of an increased complexity. ECMs are used by Jiang et al. (2014) and Zhang et al. (2017) to represent the cell behaviour, where different cost functions are designed to achieve optimal charging efficiency or minimum charging loss while charging faster. ECMs can model the charging loss by internal resistance and current rate but are not able to capture important internal state information, such as solid and electrolyte potential, ion concentration, reaction flux and side reactions that leads to Solid-Electrolyte-Interphase (SEI) growth. As a result, EMs have gained popularity. Among these, the most popular models are the Pseudo-Two-Dimensional (P2D) model introduced by Doyle, Fuller, and Newman (Doyle et al., 1993) and the Single-Particle Model (Suthar et al., 2014) that is obtained from a simplification of the former. These models are described by Partial Differential Algebraic Equations (PDAEs), which require model simplifications for numerical implementation (see e.g. Torchio et al. (2016)). However, these models have to be extended to incorporate ageing dynamics and to predict the temperature, ion concentration distribution or overpotential, in order to be used for fast-charging strategies as in Perez et al. (2016) with an SPM. In addition, side-reaction models have been used together with a DFN in Khalik et al. (2020) and Lucia et al. (2017). Unfortunately, in general the complexity of these models prevent them from being used for optimal real-time control. Due to the complexity and high dimensionality of Li-ion battery models, simplified models are often used in the context of optimal control to enable efficient computation and to make the control strategy practical for real-time implementation.

In this paper, we present an online optimal-control-based method for ageing-aware charging, where the side reaction is minimised for a given charging time, subject to several ageing-related constraints. For this purpose, similarly to what is done by (Pozzi et al., 2018), a shrinking-horizon model-predictive control is implemented, which uses a surrogate model presented in Khalik et al. (2021). The latter is used to approximate the states of the DFN model that are correlated with ageing and combines a black-box Finite-Dimensional Linear-Time-Invariant (FD-LTI) model and a static nonlinear model which is state-of-charge dependent. Note that the shrinking-horizon technique relies on accurate battery models for optimization. Moreover, in order to close the feedback control loop, a Kalman filter with forgetting factor is used (Beelen et al., 2020). The effectiveness of this strategy is demonstrated with a Pareto-front analysis. Summarizing, the content of this work consists of i) A Model Predictive Control (MPC) ageing-aware strategy for charging; ii) a shrinking-horizon approach which allows for reducing the prediction horizon as the cell charges; iii) the application of a Kalman filter with forgetting factor as a state observer to the surrogate model.

The paper is organized as follows: Section 2 presents the modelling approach, while Section 3 discusses the optimal control problem formulation, the state observer, and the algorithm. The results are presented in Section 4, and the conclusions are drawn in Section 5.

2. BATTERY MODELLING

In this section, we present the Li-ion battery cell modelling, starting with the DFN model, which is used as the "real plant" in this paper's simulations. We then introduce the surrogate modelling method proposed in Khalik et al. (2021), which is an approximation of the ageing-related DFN model states used in the controller.

2.1 Doyle-Fuller-Newman Model

The Pseudo-Two-Dimensional (P2D) model (Doyle et al., 1993), commonly known as the Doyle-Fuller-Newman (DFN) model, is the most extensively used electrochemical model and it is described by Partial Differential Algebraic Equations (PDAEs). In this section, we just briefly discuss the four major PDAEs and the equation representing the side reaction. We direct the reader to (Khalik et al., 2020) for definitions of the numerous variables and boundary conditions that characterise the primary reactions. Note that in the following the time and spatial dependence of the provided variables will not be included in the equations for simplicity reasons.

Fick's law provides the Li-ion concentration in the solid phase $c_s(x, r, t)$

$$\frac{\partial c_s}{\partial t} = \frac{D_s}{r^2}\frac{\partial}{\partial r}\left(r^2\frac{\partial c_s}{\partial r}\right), \tag{1}$$

for $x \in [0, \delta_n] \cup [L - \delta_p, L]$, where D_s is the solid diffusion coefficient and r is the radial direction along which the ions intercalate within the active particles. The thicknesses of the negative and positive electrodes are denoted with δ_n and δ_p respectively, whereas L models the thickness of the cell.

For $x \in [0, L]$, the Li-ion concentration in the electrolyte phase $c_e(x, t)$ is given by

$$\epsilon_e\frac{\partial c_e}{\partial t} = \frac{\partial}{\partial x}\left(D_e\frac{\partial c_e}{\partial x}\right) + \alpha_s(1 - t_+^0)j_n, \tag{2}$$

with $j_n = j_1 + j_2$, where j_1 is the main-reaction flow as determined by the standard Butler-Volmer equation and j_2 is the side-reaction flux as described later in this section. The diffusion coefficient within the electrolyte is denoted with D_e, the transference number is t_+^0 and finally α_s is the particle surface-area-to-volume.

Ohm's law gives the potential in the solid phase $\phi_s(x,t)$ for $x \in [0, \delta_n] \cup [L-\delta_p, L]$, i.e.,

$$\frac{\partial}{\partial x}\left(\sigma^{\text{eff}}\frac{\partial \phi_s}{\partial x}\right) = \alpha_s F j_n, \tag{3}$$

where σ_{eff} is the effective solid-phase conductivity and F the Faraday constant.

The potential in the electrolyte phase $\phi_e(x,t)$ for $x = [0, L]$ is given by

$$\frac{\partial}{\partial x}\left(\kappa_{\text{eff}}\frac{\partial \phi_e}{\partial x} + \kappa_{\text{eff}}\frac{2RT}{F}(t_+^0 - 1)\frac{\partial \ln c_e}{\partial x}\right) = -\alpha_s F j_n, \tag{4}$$

where κ_{eff} is the effective electrolyte conductivity, T is the cell temperature and R is the universal gas constant.

The electrochemical reaction rate of the Li-ion-consuming side reaction is only defined for $x \in [0, \delta_n]$ and is assumed to be zero elsewhere, as indicated by

$$j_2 = -\frac{i_{0,2}}{F}\exp\left(-\frac{2\alpha_{c,2}F}{RT}\eta_2\right), \tag{5}$$

with $i_{0,2}$ is the exchange current density of the side reaction and $\alpha_{c,2}$ denotes the cathodic transfer coefficient. The side-reaction overpotential η_2 is given by

$$\eta_2 = \phi_s - \phi_e - U_2 - FR_f j_n, \tag{6}$$

where U_2 is is the equilibrium potential of the side reaction, which is usually assumed to be a constant, while R_f defines the film resistance.

Eventually, the quantity of charge lost Q_l due to Li-ion loss as a result of side reaction in the negative electrode is calculated as

$$\frac{dQ_l}{dt} = -\alpha_s A_{\text{surf}} F \int_0^{\delta_n} j_2 dx, \tag{7}$$

where A_{surf} is the area of the electrode surface.

2.2 Surrogate modelling approach

In this part, we provide an introduction to the surrogate modelling approach proposed by (Khalik et al., 2021). The latter is used to approximate ageing-related DFN model states. In particular, the surrogate model in this work combines a static nonlinear state-of-charge-dependent model with a black-box FD-LTI model.

Figure 1 illustrates the surrogate modelling method as an input/output model, where the applied current serves as the input and the predicted voltage and virtual outputs represent the relevant part of the unmeasurable DFN model states. These virtual outputs capture the essential states of the DFN that cannot be directly measured in a real battery cell. The vector $\mathbf{y}$ of virtual outputs and the terminal voltage of the cell can be seen as the sum of the output of an FD-LTI model $\bar{\mathbf{y}}$ and a SOC-dependent static model $\mathbf{h}(s)$, with s denoting the SOC for brevity. This can be described in a discrete-time representation as

$$\mathbf{y}_k = \bar{\mathbf{y}}_k + \mathbf{h}(s_k), \tag{8}$$

with k the discrete time instant. The SOC is computed by the Coulomb counting equation as

$$s_{k+1} = s_k + \frac{\delta_t I_k}{C_b}, \tag{9}$$

where δ_t is the sampling time, I_k is the input current at time $k\delta_t$ and C_b is the reversible cell battery capacity.

The FD-LTI model is an AutoRegressive Exogenous (ARX) model with one input I_k and n_y outputs. The one-step-ahead prediction that produces an estimate $\hat{\mathbf{y}}_k$ can be expressed as

$$\hat{\mathbf{y}}_k = \mathbf{B}_{\text{ARX}}(q,\boldsymbol{\theta})I_k - \mathbf{A}_{\text{ARX}}(q,\boldsymbol{\theta})\bar{\mathbf{y}}_k, \tag{10}$$

with q the forward shift operator $I_{k-1} = (q^{-1})I_k$, and $\boldsymbol{\theta}$ are the parameters of the ARX model. In addition, in (10), $\mathbf{A}_{\text{ARX}}$ is an $n_y \times n_y$ matrix of polynomials of q^{-1}, where the polynomials have a delay of at least one sample, that is, they start with zero, and $\mathbf{B}_{\text{ARX}}$is a $n_y \times 1$ matrix of polynomials of q^{-1}, where the polynomials are monic, that is, the leading coefficients are 1. The order of the polynomials $\mathbf{A}_{\text{ARX}}$ and $\mathbf{B}_{\text{ARX}}$ is expressed by the matrices $\mathbf{N}_A \in \mathbb{R}^{n_y \times n_y}$ and $\mathbf{N}_B \in \mathbb{R}^{n_y \times 1}$ respectively. Given a specific decision for these latter matrices, as well as data from the DFN model simulation, the parameters of the ARX model can be derived by minimising a least-squares criterion of the form

$$\sum_{k\in\mathcal{K}} ||\bar{\mathbf{y}} - \hat{\mathbf{y}}(\boldsymbol{\theta})||^2, \tag{11}$$

for $k \in \mathcal{K} = \{0, 1, ..., K-1\}$, where $K = t_f/\delta_t$ is the time horizon, and $\hat{y}_k$ can be estimated from the measurements y_k using (8), providing that $\mathbf{h}(s_k)$ is known. Note that system (8)-(10) can be expressed also in a state-space form as it follows

$$\begin{cases} \mathbf{x}_{k+1} = \mathbf{A}\mathbf{x}_k + \mathbf{B}I_k \\ \quad \mathbf{y}_k = \mathbf{C}\mathbf{x}_k + \mathbf{D}I_k + \mathbf{h}(s_k), \end{cases} \tag{12}$$

with $\mathbf{x} = [s\ \bar{\mathbf{x}}]$, $\mathbf{A} = \text{diag}(1, \bar{\mathbf{A}})$, $\mathbf{B} = \begin{bmatrix}\delta_t/C_b\ \bar{\mathbf{B}}\end{bmatrix}$, $\mathbf{C} = \begin{bmatrix}\mathbf{0}\ \bar{\mathbf{C}}\end{bmatrix}$ and $\mathbf{D} = \bar{\mathbf{D}}$, where $\bar{\mathbf{x}}$, $\bar{\mathbf{A}}$, $\bar{\mathbf{B}}$, $\bar{\mathbf{C}}$ and $\bar{\mathbf{D}}$ are derived from a state-space representation of (10).

In this paper, only a combination of quantities related to the DFN has been chosen as virtual outputs to define the surrogate model. In particular, given the purpose of providing an optimal aging-aware charging strategy, only some states of the DFN are associated with aging, that are $\bar{\eta}_2(t) = \eta_2(t, \delta_n)$, $\bar{s}_n(t) = s_n(t, \delta_n)$, $\bar{s}_p(t) = s_p(t, L-\delta_p)$, $\bar{c}_{e,0} = c_e(t, 0)/c_{e,\alpha}$, $\bar{c}_{e,L} = c_e(t, L)/c_{e,\alpha}$, where $c_{e,\alpha}$ is the average electrolyte concentration. Moreover, the DFN data used for identifying the surrogate model include not only the virtual outputs but also the voltage V_t as highlighted in Figure 1. For further details on the choice of the DFN states of relevance, we refer the reader to Khalik et al. (2021).

3. OPTIMAL AGEING-AWARE STRATEGY

In this section, we describe our approach to ageing-aware charging, which balances the trade-off between battery ageing and charging time. To achieve this, we use a Shrinking-Horizon Model-Predictive Control that solves an optimal control problem based on a surrogate model outlined in Section 2. The objective is to minimize Li-ion loss due to side reactions during charging, subject to input and output constraints, within a specified charging time. It is important to note that fast charging and ageing reduction are typically competing objectives, and our approach aims to find a Pareto-optimal solution. In this scenario, the "shrinking" adaptation is required since the horizon available to take control actions shrinks as the battery charges. The control problem is written in this case so that ageing is minimised for a given charging

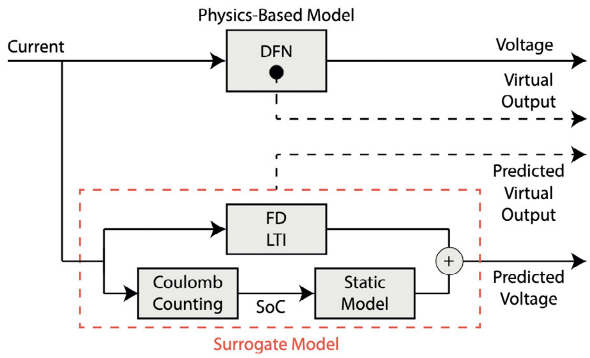

Fig. 1. Schematic illustration of the surrogate modelling approach, which approximates the outputs of a Doyle-Fuller Newman (DFN) model using a mix of a FD-LTI model and a static model (Khalik et al., 2021).

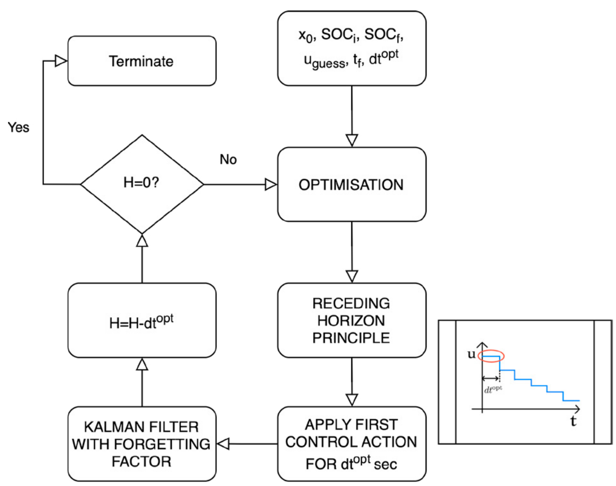

Fig. 2. Closed-loop optimal ageing-aware control strategy.

time. To effectively address this optimal-control problem a sequential-quadratic-programming (SQP) approach is used. In addition, a state observer is required to close the loop. The Kalman Filter with forgetting factor developed by Beelen et al. (2020) is employed for this purpose.

The methodology is summarized in Figure 2. In the following we first formulate the problem of optimal control for the ageing-aware charging method, then describe the resolution method and the state observer used.

3.1 Problem Formulation

We investigate the problem formulation in which the Li-ion loss related to side reactions Q_l in (7) is minimised within a certain charging time t_f, with the integral $\int_0^{\delta_n} j_2 dx$ that is simplified to $j_2(\delta_n, t)$, such that

$$\min_{x_k, I_k} \quad Q_l(x_k, I_k) = \sum \alpha_1 \exp(\alpha_2 \eta_{2,k}(x_k, I_k)) \tag{13}$$

$$\text{s.t.} \quad \text{state dynamics (12)} \quad \forall k \in \mathcal{K} = \{0, 1, \ldots, K\}$$

$$I_{\min} \leq I_k \leq I_{\max} \tag{14}$$

$$y_{\min} \leq y_k \leq y_{\max} \tag{15}$$

$$s_K = s_0 + \frac{\delta_t}{C_b} \sum_{k \in \mathcal{K}} I_k \geq s_f \tag{16}$$

where $\alpha_1 = i_{0,2} \alpha_s A_{\text{surf}} \delta_t \delta_n$, $\alpha_2 = \frac{-2\alpha_{c,2}F}{RT}$ and $\eta_2(x_k, I_k) = C_2 x_k + D_2 I_k + h_2(s_k)$ with C_2, D_2 and $h_2(s_k)$ denoting the second row of C, D and h respectively. The cost function (13) is subjected to the input (14) and output (15) constraints. Finally, there is a minimum-stored-charge constraint described by (16) for a specified initial SOC s_0 and a desired final SOC s_f.

3.2 State Observer

An Extended Kalman Filter with cross-correlated noise and forgetting factor is used in this paper as a state observer. The forgetting factor can be implemented in estimation schemes to increase the relevance of new observations over previous ones. In particular, the new data are assumed to be exponentially (by a γ factor) more relevant than the old data. Let consider the linear time-varying system

$$\begin{cases} \mathbf{x}_{k+1} = \mathbf{A}\mathbf{x}_k + \mathbf{B}I_k + \tilde{\mathbf{w}}_k \\ \mathbf{y}_k = \mathbf{C}\mathbf{x}_k + \mathbf{D}I_k + \tilde{\mathbf{v}}_k, \end{cases} \tag{17}$$

with $\tilde{\mathbf{w}}_k = \mathbf{G}_k[\mathbf{w}_k^{\mathrm{T}}, \mathbf{v}_k^{\mathrm{T}}]^{\mathrm{T}}$ and $\tilde{\mathbf{v}}_k = \mathbf{M}_k[\mathbf{w}_k^{\mathrm{T}}, \mathbf{v}_k^{\mathrm{T}}]^{\mathrm{T}}$. We assume that $\mathbb{E}[\mathbf{w}_k \mathbf{w}_k^{\mathrm{T}}] = 1$, $\mathbb{E}[\mathbf{v}_k \mathbf{v}_k^{\mathrm{T}}] = 1$ and $\mathbb{E}[\mathbf{w}_k \mathbf{v}_k^{\mathrm{T}}] = 0$ such that

$$\mathbb{E}\left[\begin{bmatrix} \tilde{\mathbf{w}}_k \\ \tilde{\mathbf{v}}_k \end{bmatrix} \begin{bmatrix} \tilde{\mathbf{w}}_k \\ \tilde{\mathbf{v}}_k \end{bmatrix}^{\mathrm{T}}\right] = \begin{bmatrix} \mathbf{Q}_k & \mathbf{S}_k \\ \mathbf{S}_k & \mathbf{R}_k \end{bmatrix} = \begin{bmatrix} \mathbf{G}_k \mathbf{G}_k^{\mathrm{T}} & \mathbf{G}_k \mathbf{M}_k^{\mathrm{T}} \\ \mathbf{M}_k \mathbf{G}_k^{\mathrm{T}} & \mathbf{M}_k \mathbf{M}_k^{\mathrm{T}} \end{bmatrix}, \tag{18}$$

where $\mathbf{Q}_k$ and $\mathbf{R}_k$ are the (time-varying) process-noise covariance and measurement-noise covariance of the noises $\tilde{\mathbf{w}}_k$ and $\tilde{\mathbf{v}}_k$, respectively. $\mathbf{S}_k$ denotes the cross correlation between the noises $\tilde{\mathbf{w}}_k$ and $\tilde{\mathbf{v}}_k$. The main informations useful for understanding the Kalman Filtering implementation for (17) are here illustrated. To produce an EKF implementation, the state equations are linearized at each time instant k. Moreover, for further information, the reader is referred to (Beelen et al., 2020). The state estimation framework consists of two steps. In the first one, the measurement update, returns

$$\mathbf{L}_k = \tilde{\mathbf{P}}_k^+ + \mathbf{C}_k^{\mathrm{T}}(\mathbf{C}_k^{\mathrm{T}} \tilde{\mathbf{P}}_k^+ + \mathbf{C}_k + \gamma \mathbf{R}_k)^{-1}, \tag{19}$$

$$\hat{\mathbf{x}}_{k+1}^- = \hat{\mathbf{x}}_k^+ + \mathbf{L}_k(\mathbf{y}_k - \mathbf{C}_k \hat{\mathbf{x}}_k^+ - \mathbf{D}_k I_k), \tag{20}$$

$$\tilde{\mathbf{P}}_{k+1}^- = \frac{1}{\gamma}(\mathbf{I} - \mathbf{L}_k \mathbf{C}_k)\tilde{\mathbf{P}}_k^+, \tag{21}$$

while in the second phase the time update computes the final estimate

$$\hat{\mathbf{x}}_{k+1}^+ = \mathbf{A}_k \hat{\mathbf{x}}_{k+1}^- + \mathbf{B}_k I_k + \mathbf{S}_k \mathbf{R}_k^{-1}(\mathbf{y}_k - \mathbf{C}_k \hat{\mathbf{x}}_{k+1}^+ - \mathbf{D}_k I_k), \tag{22}$$

$$\tilde{\mathbf{P}}_{k+1}^+ = (\mathbf{A}_k - \mathbf{S}_k \mathbf{R}^{-1} \mathbf{C}_k) \tilde{\mathbf{P}}_{k+1}^- (\mathbf{A}_k - \mathbf{S}_k \mathbf{R}^{-1} \mathbf{C}_k)^{\mathrm{T}} + \mathbf{Q}_k - \mathbf{S}_k \mathbf{R}^{-1} \mathbf{S}_k^{\mathrm{T}} \tag{23}$$

where $\gamma \leq 1$ is the forgetting factor that is chosen close to 1 usually.

4. RESULTS

The proposed strategy is tested in simulation in this section, using the surrogate model for control and the more accurate DFN model as the "real" battery to achieve a realistic scenario.

4.1 Validation of the surrogate model

The surrogate model is provided by Khalik et al. (2021), where $\mathbf{y}_k$ and $\mathbf{h}(s_k)$ are given in (8). The ARX model is parameterized in MATLAB using the System Identification Toolbox, where the matrices $\mathbf{N}_A$ and $\mathbf{N}_B$ were chosen to create a suitable balance between model accuracy and model complexity, and are provided by

$$\mathbf{N}_A = \begin{bmatrix} 0 & 1 & 1 & 1 & 1 & 1 \\ 0 & 1 & 1 & 1 & 0 & 1 \\ 0 & 1 & 1 & 0 & 1 & 0 \\ 0 & 1 & 0 & 2 & 1 & 0 \\ 0 & 1 & 1 & 0 & 1 & 1 \\ 0 & 1 & 0 & 1 & 1 & 1 \end{bmatrix}, \quad \mathbf{N}_B = \begin{bmatrix} 2 \\ 2 \\ 2 \\ 2 \\ 1 \\ 1 \end{bmatrix}. \tag{24}$$

The DFN model can be simulated with a selected current profile to provide data from which the ARX model (10) can be parameterized using the least-squares criterion (11). This parameterization will be done in two phases as it is detailed in Khalik et al. (2021).

Figure 3 displays the validation results of the surrogate model using a 100min charging current profile. The trajectories of the surrogate model's virtual outputs, voltage, and j_2 are plotted in blue, while the DFN's corresponding trajectories are in red. Despite a noticeable mismatch between the two models, this is acceptable when considering the computational advantage provided by the surrogate model.

4.2 Pareto-front analysis

In this paper, we consider the closed-loop optimal-control-based ageing-aware charging method described in Section 3. Constraints have been placed on the outputs which are composed of the set of virtual outputs and the terminal voltage of the cell. Specifically, we have $\bar{s}_{n,\max} = 0.93$, $\bar{s}_{n,\min} = 0.52$, $\bar{c}_{e,\max} = 1.27$ and $\bar{c}_{e,\min} = 0.85$. Note that these values are chosen artificially. Ideally they should be selected in the least restrictive manner to prevent unmodelled ageing phenomena of the battery cell.

To ensure that the optimal-control problem can be implemented in real-time, we have fixed the number of optimal variables to $n = 100$, resulting in an optimization step size of $\delta_t^{\text{opt}} = t_f/n$. The simulation sampling time is set to 1 second. The SOC range considered for the simulation setup is from $s_0 = 0.2$ to $s_f = 0.9$.

Figure 4 shows the Pareto-fronts achieved with different optimal-control-based methods. In particular, we tested the closed-loop strategy proposed in this paper with three different values of the forgetting factor, i.e. $\gamma \in \{0.995, 0.999, 1\}$. Then we compare these results with the Pareto-fronts obtained using two open-loop optimal control strategies, the first one (offline surrogate) proposed in (Khalik et al., 2021) adopts the same surrogate model while the second one (offline DFN) employs the DFN model used also for simulating the "real" plant as it is performed in (Khalik et al., 2020). Note that the latter one is shown as a benchmark because it uses the same model for the optimisation and the "real" battery. Several comments can be made regarding this figure. First of all the surrogate model is a large simplification of the DFN and therefore even more than reality. Therefore, the optimal control method based on this model is shown to be more effective if used in a closed-loop with an MPC strategy with a shrinking-horizon. Note that the offline surrogate strategy is demonstrated to be better than the CC-CV and multistage protocols standards as analysed in Khalik et al. (2021). By varying γ from 1 (pure Kalman Filter) towards lower values, the performances improve, i.e. given a charging time we have a lower degradation of the cell. For $\gamma = 0.995$ we even notice an improvement concerning what we assume to be our optimality benchmark, i.e. solving the optimization problem with the true model. This is actually due to the fact that the problem is non-convex and in the specific case, the open-loop case, using the DFN model for optimisation, has found a local solution. This is demonstrated by the fact that by varying the initial guess and putting them equal to the optimal solution found with $\gamma = 0.995$, we see a further improvement of the Pareto-front for the open-loop with the DFN model case (offline DFN*). Note that although, as we expect, the open-loop DFN case yields the best achievable curve, it exhibits an increasing behaviour over time. This is due to the fact that to make the method effectively implementable in real-time, the number of optimization variables has been kept constant, and not the step size. This means that for longer charging times, the optimization step size is greater and therefore the current profile has longer constant intervals.

4.3 Influence of the forgetting factor on the state observer

Figures 5 and 6 show the trends of the state of charge and the voltage across the cell, for a charging time $t_f = 67$min. It can be seen how as the γ value decreases, the SOC estimate worsens at the expense of better tracking of the voltage measurements. Although the surrogate model has been identified starting from the DFN model, with the open-loop optimization the final SOC is not achieved with precision. Furthermore, the estimate of the voltage made with the surrogate model in an open-loop differs more from the voltage of the "real plant".

4.4 Comparison of charging profiles

In this work we considered two cases: a first scenario where only a lower bound on the current has been considered ($I_{\min} = 0$) and a second case in which also an upper bound is taken into account ($I_{\max} = 1C$).

Figure **??** shows the optimal current profiles always obtained for $t_f = 67$min. The optimizations made with the surrogate model return different current profiles in open-loop and closed-loop. The main differences in those profiles are evident especially at both ends of the time interval. The offline surrogate strategy yields higher currents that result in a worse Pareto-front, i.e. worse performance in terms of ageing. Figure 8 exhibits the effect of the upper bound on the current. In this case the current profiles are limited to the upper bound value at the start of charging. This inevitably limits the effect of lowering the degradation of the cell.

5. CONCLUSIONS

This study has presented a closed-loop-control-based strategy for ageing-aware charging. A surrogate model that

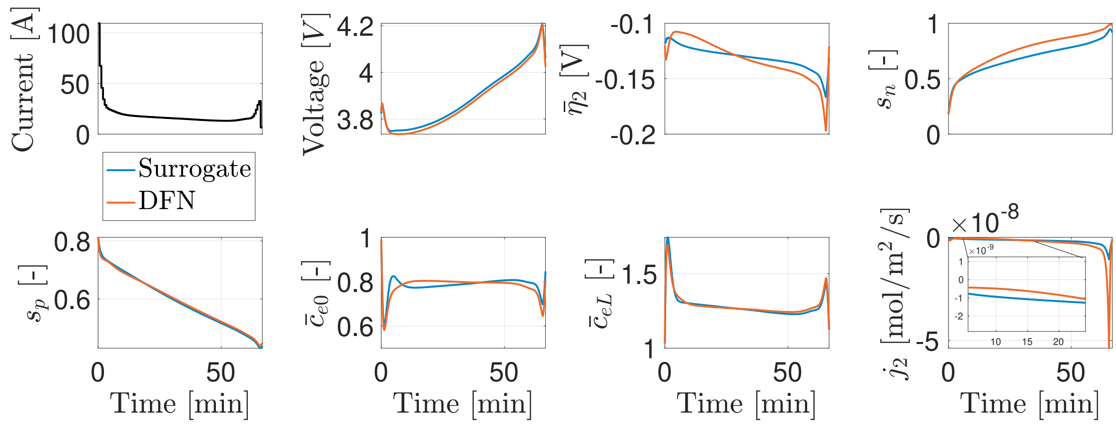

Fig. 3. Validation of the surrogate model with the DFN model.

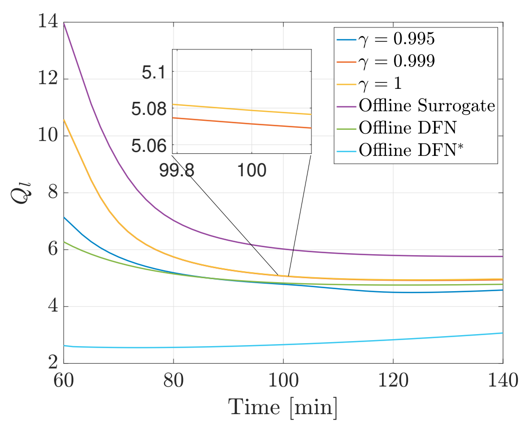

Fig. 4. Trade-off between charging time and Li-ion loss (Q_l) for different ageing-aware charging techniques evaluated from 60 to 140 minutes.

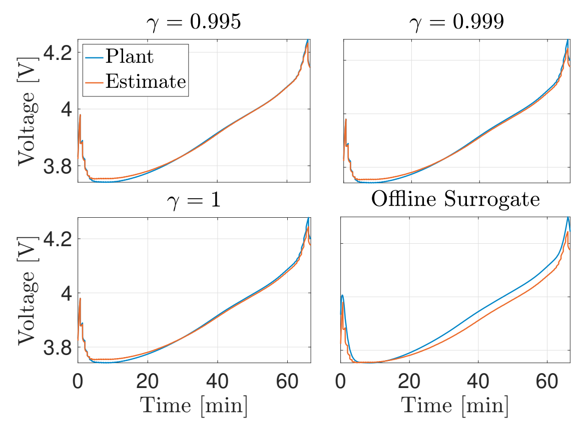

Fig. 6. DFN voltage (red) and estimated voltage (blue) using the Kalman Filter with specified forgetting factors γ and simulating (17) for open-loop (bottom-right) during a 67-minute charging duration.

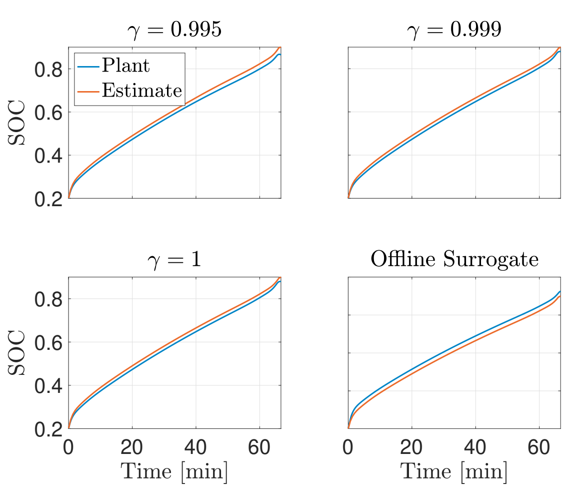

Fig. 5. DFN state of charge (red) and estimated state of charge (blue) using the Kalman Filter with specified forgetting factors γ and simulating (17) for open-loop (bottom-right) during a 67-minute charging duration.

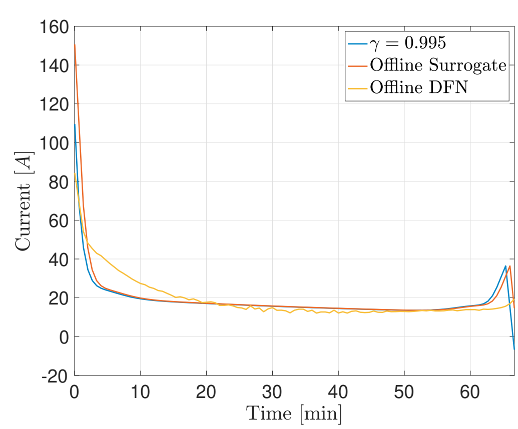

Fig. 7. Current profiles for different ageing-aware charging methods obtained during a 67-minute charging time.

combines a linear-time-invariant model and a nonlinear model has been used to approximate ageing-related DFN model states. A shrinking-horizon approach has been employed to reduce the prediction horizon as the cell charges. A Kalman filter with a forgetting factor has been used as a state observer. The methodology has been demonstrated to be effective in minimizing capacity loss compared to open-loop optimization in simulations using a DFN as a “real plant”. Varying the forgetting factor γ showed a

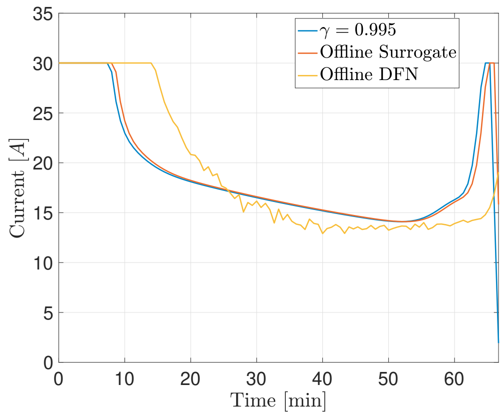

Fig. 8. Current profiles for different ageing-aware charging methods obtained during a 67-minute charging time at $I_{\max} = 1C$.

significant reduction in Q_l for lower γ values, giving more importance to reducing the mismatch between measured and estimated outputs.

REFERENCES

Beelen, H., Bergveld, H.J., and Donkers, M. (2020). Joint estimation of battery parameters and state of charge using an extended kalman filter: a single-parameter tuning approach. *IEEE Transactions on Control Systems Technology*, 29(3), 1087–1101.

Bhardwaj, R.C., Hwang, T., and Mank, R.M. (2014). Modulated, temperature-based multi-cc-cv charging technique for li-ion/li-polymer batteries. US Patent 8,816,648.

Doyle, M., Fuller, T.F., and Newman, J. (1993). Modeling of galvanostatic charge and discharge of the lithium/polymer/insertion cell. *Journal of the Electrochemical society*, 140(6), 1526.

Jiang, J., Liu, Q., Zhang, C., and Zhang, W. (2014). Evaluation of acceptable charging current of power li-ion batteries based on polarization characteristics. *IEEE Transactions on Industrial Electronics*, 61(12), 6844–6851.

Jiang, L., Li, Y., Huang, Y., Yu, J., Qiao, X., Wang, Y., Huang, C., and Cao, Y. (2020). Optimization of multi-stage constant current charging pattern based on taguchi method for li-ion battery. *Applied Energy*, 259, 114148.

Khalik, Z., Bergveld, H.J., and Donkers, M. (2020). Ageing-aware charging of lithium-ion batteries using an electrochemistry-based model with capacity-loss side reactions. In *2020 American Control Conference (ACC)*, 2213–2218. IEEE.

Khalik, Z., Bergveld, H.J., and Donkers, M. (2021). Ageing-aware charging of lithium-ion batteries using a surrogate model. In *2021 American Control Conference (ACC)*, 4414–4420. IEEE.

Khan, A.B. and Choi, W. (2018). Optimal charge pattern for the high-performance multistage constant current charge method for the li-ion batteries. *IEEE transactions on energy conversion*, 33(3), 1132–1140.

Lee, Y., Jeghan, S.M.N., and Lee, G. (2021). Boost charging lithium-ion battery using expanded graphite anode with enhanced performance. *Materials Letters*, 299, 130077.

Li, J., Murphy, E., Winnick, J., and Kohl, P.A. (2001). The effects of pulse charging on cycling characteristics of commercial lithium-ion batteries. *Journal of Power Sources*, 102(1-2), 302–309.

Lucia, S., Torchio, M., Raimondo, D.M., Klein, R., Braatz, R.D., and Findeisen, R. (2017). Towards adaptive health-aware charging of li-ion batteries: A real-time predictive control approach using first-principles models. In *2017 American Control Conference (ACC)*, 4717–4722. IEEE.

Perez, H.E., Hu, X., and Moura, S.J. (2016). Optimal charging of batteries via a single particle model with electrolyte and thermal dynamics. In *2016 American Control Conference (ACC)*, 4000–4005. IEEE.

Pozzi, A., Torchio, M., and Raimondo, D.M. (2018). Assessing the performance of model-based energy saving charging strategies in li-ion cells. In *2018 IEEE Conference on Control Technology and Applications (CCTA)*, 806–811. IEEE.

Suthar, B., Northrop, P.W., Braatz, R.D., and Subramanian, V.R. (2014). Optimal charging profiles with minimal intercalation-induced stresses for lithium-ion batteries using reformulated pseudo 2-dimensional models. *Journal of The Electrochemical Society*, 161(11), F3144.

Torchio, M., Magni, L., Gopaluni, R.B., Braatz, R.D., and Raimondo, D.M. (2016). Lionsimba: a matlab framework based on a finite volume model suitable for li-ion battery design, simulation, and control. *Journal of The Electrochemical Society*, 163(7), A1192.

Zhang, C., Jiang, J., Gao, Y., Zhang, W., Liu, Q., and Hu, X. (2017). Charging optimization in lithium-ion batteries based on temperature rise and charge time. *Applied energy*, 194, 569–577.